

Finite element modeling of non-ductile RC walls



A.S. Gebreyohannes, G.C. Clifton & J.W. Butterworth

The University of Auckland, New Zealand

SUMMARY:

A three-dimensional finite-element model developed to undertake a study of the behaviour of non-ductile reinforced concrete walls when subjected to earthquake induced lateral forces is presented. The adopted modelling approach and the solution controls implemented for the non-linear finite-element analyses are discussed in detail. The model was verified using data obtained from an experimental program that involved testing of specimens that were replicas of wall segments of an existing building.

The outcomes of the analyses indicate that the developed model is capable of predicting the initial stiffness, the stiffness degradation, the lateral force capacity and the strength degradation characteristics of non-ductile walls to a good accuracy. A sensitivity study revealed that the response of this type of wall is not significantly affected by the adopted concrete material parameters. In addition, it was observed that assuming an elasto-plastic material behaviour for the reinforcement of the test specimens results in prediction of lower bound response that is in good agreement with that determined experimentally.

Keywords: Numerical modelling, finite element method, reinforced concrete, non-ductile walls

1 INTRODUCTION

The finite element (FE) study presented herein was based on the reinforced concrete (RC) walls of an existing building located in Wellington, New Zealand. The street corner building was constructed in 1928 before the publishing of NZSS 95 (NZ Standards Institute, 1935) that introduced seismic resistant design requirements for the first time in New Zealand. The building was assessed in accordance with the non-linear dynamic procedure (ASCE/SEI 41, 2007) to determine its likely performance when subjected to a design level earthquake excitation. From the assessment it was found that the capacity of the building will be exceeded in a *moderate* level earthquake, which is defined as being one-third as strong as the design level earthquake relevant to the building site (DBH, 2004). The non-ductile RC walls of the building were identified as the primary lateral force resisting components of the building (Gebreyohannes et al., 2012a).

In order to obtain an understanding of the seismic performance of the walls that were found in the case study building, an experimental test was undertaken on replicas of typical segments of the most critical walls. The walls are singly reinforced with widely spaced plain round bars providing a quantity of longitudinal and transverse reinforcement that is much less than that required by current design standards such as ACI 318-11 (ACI Committee 318, 2011) and NZS 3101 (Standards NZ, 2006) to induce a ductile response. The longitudinal reinforcing bars are typically spliced just above the floor levels. The spliced bars lack proper end anchorages and the splice lengths are too short according to current design standards (ACI Committee 318, 2011, Standards NZ, 2006) to initiate yielding of the spliced bars before relative slip occurs. There is also a lack of transverse confinement reinforcement to contain concrete in compression zones and to prevent longitudinal reinforcing bars from buckling.

2 SUMMARY OF THE EXPERIMENTAL STUDY

Twelve full-scale wall components were constructed in-situ and experimentally tested under cyclic quasi-static loading, as part of a research program planned to assess the seismic performance of existing buildings in New Zealand. The geometric characteristics and reinforcing bar configurations of the test specimens were determined based on the original structural drawings and construction specifications of the case study building. The dimensions and reinforcing bar arrangements of the eight test specimens discussed herein are presented in **Figure 1**. The material properties are summarized in **Table 1**.

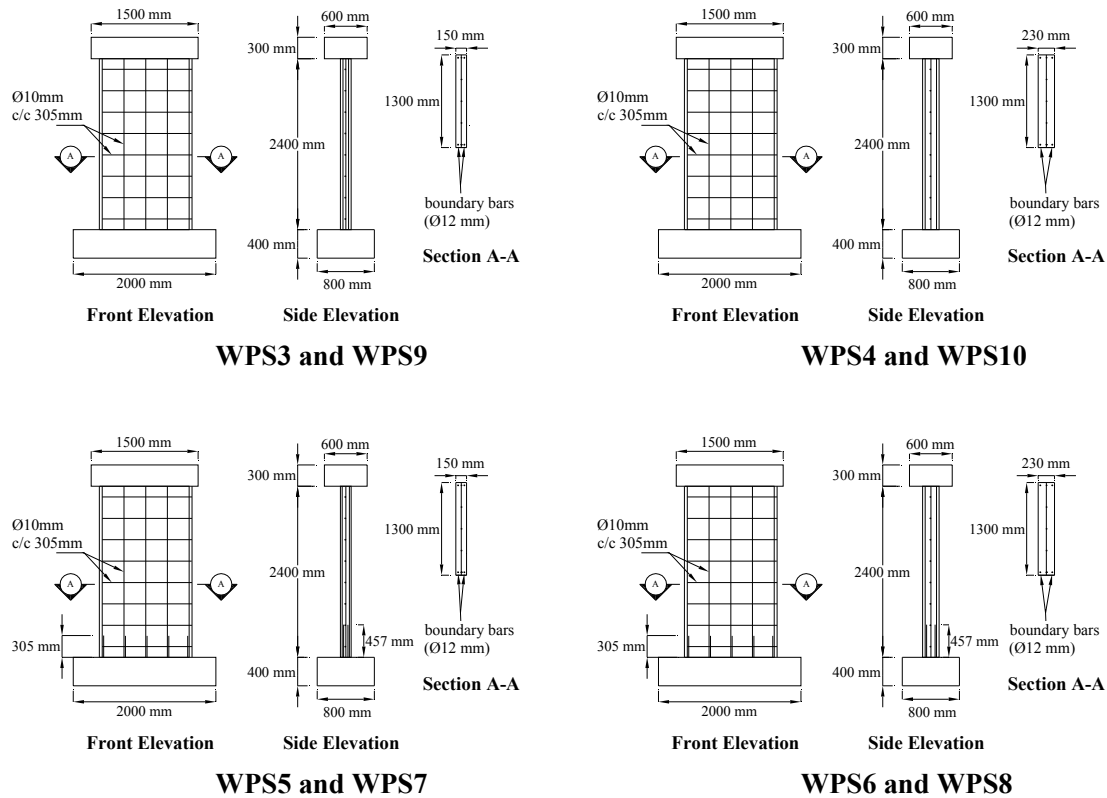


Figure 1. Test specimen geometries and reinforcement details

The longitudinal reinforcing bars were spliced near the base of the walls in four of the test specimens (specimens WPS5 to WPS8), whereas in the remaining four test specimens the longitudinal reinforcing bars were continuous and were anchored outside the walls. The test specimens were subjected to a reverse bending loading condition using a steel loading beam mounted on and anchored to the top RC blocks (See **Figure 2(a)**). The double bending loading condition was representative, as closely as possible, of the fixed-fixed sway support condition of wall components in multi-storey buildings. Compressive axial load was applied to the walls using four high strength bars that were positioned parallel to the wall centerline and anchored to the strong floor (Refer to **Figure 2(a)**).

The experimental study revealed that the lateral force resisting capacity of this type of wall is limited by its flexural strength. Yielding of the longitudinal reinforcement dictates the strength, due to the low quantity of reinforcing bars present in the walls. The strength and the stiffness of the walls degrade rapidly and significantly. The walls also exhibit limited energy dissipation capacity, principally due to a lack of any dissipative mechanism except friction at the wall foundation interfaces after the longitudinal reinforcing bars have ruptured.

During experimental testing, strain gauges were glued to the longitudinal reinforcing bars at 50 mm above the top surface of the foundation blocks and at 50 mm below the concrete loading beams.

Strains measured by the gauges revealed that the longitudinal reinforcement, even those that were spliced, were able to develop strains that were greater than but close to the experimentally determined yield strains of the bars. The measured peak strains were generally less than 2%, which is well below the fracture strain or the strain associated with developing the ultimate tensile strength of the reinforcing bars. These peak strains correspond to the level of strain developed at those locations when drop in the lateral force histories was observed and fracturing/slip of the longitudinal reinforcing bars occurred. The reader is referred to the article on the experimental study (Gebreyohannes et al., 2012b) for further details.

Table 1. Material properties

| Test specimen | f'_c MPa | Longitudinal and transverse reinforcement | | | | | Boundary reinforcement | | | Longitudinal reinforcement splices | | |
|---------------|---------------|---|----------------------|------------------|---------------|---------------|------------------------|--------------|------------------|------------------------------------|----------------------|----------------------|
| | | A_l, A_t mm | f_y, f_{yt} MPa | f_{ult} MPa | ρ_l % | ρ_t % | A_b mm | f_y MPa | f_{ult} MPa | splice | $l_b, \phi 10$ mm | $l_b, \phi 12$ mm |
| WPS3 | 19.6 | $\phi 10$ | 351 | 488 | 0.20 | 0.17 | 4 $\phi 12$ | 388 | 555 | No | - | - |
| WPS4 | 16.2 | $\phi 10$ | 351 | 488 | 0.13 | 0.11 | 4 $\phi 12$ | 305 | 436 | No | - | - |
| WPS5 | 29.4 | $\phi 10$ | 348 | 487 | 0.20 | 0.17 | 4 $\phi 12$ | 516 | 662 | Yes | 305 | 457 |
| WPS6 | 24.8 | $\phi 10$ | 348 | 487 | 0.13 | 0.11 | 4 $\phi 12$ | 516 | 662 | Yes | 305 | 457 |
| WPS7 | 21.3 | $\phi 10$ | 344 | 456 | 0.20 | 0.17 | 4 $\phi 12$ | 305 | 438 | Yes | 305 | 457 |
| WPS8 | 22.5 | $\phi 10$ | 344 | 456 | 0.13 | 0.11 | 4 $\phi 12$ | 305 | 438 | Yes | 305 | 457 |
| WPS9 | 20.2 | $\phi 10$ | 490 | 631 | 0.20 | 0.17 | 4 $\phi 12$ | 301 | 433 | No | - | - |
| WPS10 | 19.3 | $\phi 10$ | 490 | 631 | 0.13 | 0.11 | 4 $\phi 12$ | 301 | 433 | No | - | - |

Note: 1 mm = 0.0394 in.; 1 MPa = 0.145 ksi

3 THE FINITE ELEMENT MODEL

The FE model was developed in the commercial package Abaqus (Dassault Systèmes Simulia Corp., 2010). Abaqus/CAE was employed to create the numerical model of the walls, to submit and monitor an analysis job, and to view and post-process the results of the analyses. Abaqus/Explicit was used for the analyses of the walls, as analyses in Abaqus/Explicit suffer fewer convergence difficulties than do analyses in Abaqus/Standard, when highly non-linear materials like concrete are present in a model. Abaqus/Explicit employs the explicit integration scheme to solve a system of equations in very small time increments and allows models to undergo large deformations and rotations.

3.1 Geometric modeling and boundary conditions

The experimental specimens had axes of symmetry located at the mid-thickness planes of the walls (Refer to **Figure 2**). To minimize computational cost, the specimens were divided into two at their axes of symmetry and only half of the specimens were analysed. Three-dimensional solid members were used to model the foundation blocks, the walls and the top blocks. The reinforcing bars were modelled using three-dimensional truss members. The steel loading beam, the cross beams and the high strength bars that were used to apply lateral forces and axial loads were modelled using three-dimensional beam members. A three-dimensional beam member that had a length equal to the length of the hydraulic actuator was used to model the actuator. Linear spring members were used to model the coil springs that were provided underneath the strong floor to prevent the high strength bars from contributing to the stiffness and strength of the walls.

As the foundation blocks were tightly secured to the strong floor, all of the degrees of freedoms of all of the nodes of the bottom surfaces of the foundation blocks were constrained from moving. At the planes of symmetry all of the nodes were constrained from an out of plane translation and rotation about the two principal in-plane axes (Refer to **Figure 2(b)**). Kinematic coupling of all of the degrees of freedoms of the nodes was employed to connect the high strength bars to the cross beams, the cross beams to the steel loading beam, the steel loading beam to the actuator, and the steel loading beam to

the RC top block. Lateral force was applied by prescribing velocity at the tip of the actuator that was located furthest from the steel loading beam, to replicate the path that was traversed by the actuator during testing. Concentrated compressive loads were applied at the two locations on the steel loading beam where axial loads were applied.

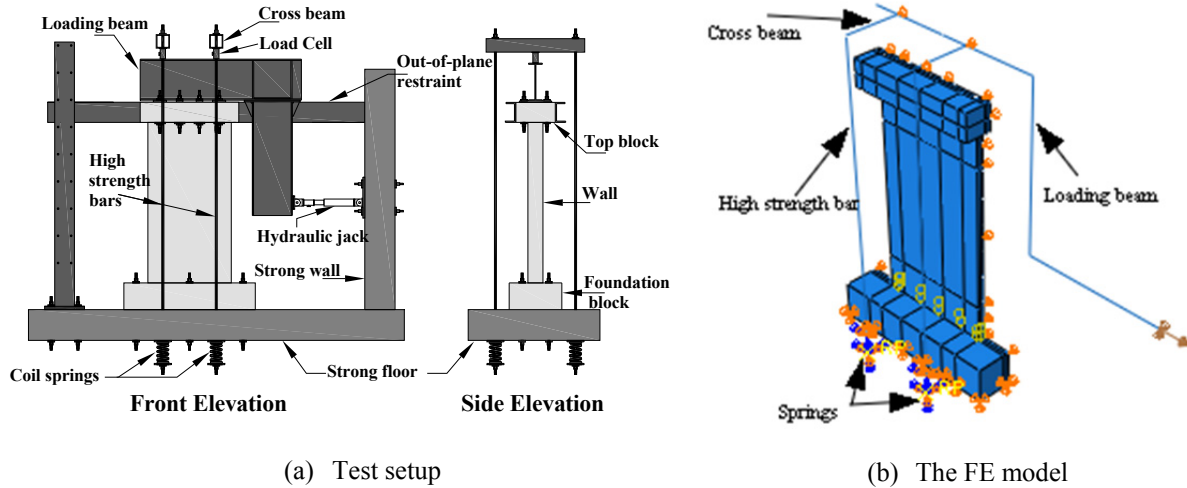


Figure 2. The experimental test setup and the FE model

3.2 Material modeling

In order to capture the behaviour of the experimentally tested walls with the FE model, the material models incorporated into the FE model had to accurately describe the properties of the constituent materials and the interactions that take place between them. Principally, the material models had to capture the stiffness and the strength degradation of concrete due to crack development, plasticity and strain at fracture of reinforcement, plasticity of plain concrete and the interaction between reinforcement and the surrounding concrete.

3.2.1 Concrete

The Concrete Damage Plasticity (CDP) model, which is available in Abaqus, was used to describe the behaviour of concrete under loading. The CDP model was developed principally for the analysis of concrete members subjected to cyclic loading. This model implements the yield functions proposed by Lubliner et al. (Lubliner et al., 1989) along with the modifications proposed by Lee and Fenves (Lee and Fenves, 1998). The concepts of isotropic damaged elasticity and hardening plasticity were employed, and concrete was assumed to fail through the mechanisms of tensile cracking and compressive crushing. The evolution of the failure surface in this model is controlled by tensile and compressive equivalent plastic strains, which are linked to the tension and compression failures respectively. The CDP model defines the behaviour of concrete under multi-axial loading conditions based on input uni-axial properties and other material properties such as Poisson's ratio (ν), dilation angle (ψ) and ratio of initial equi-bi-axial compressive yield stress to initial uni-axial compressive yield stress (σ_{b0}/σ_{co}).

The stress-strain relationship of concrete under uni-axial compression and uni-axial tension were described using compressive strength test results (Refer to **Table 1**) and provisions of CEB-FIP Model Code 90 (CEB/FIP, 1990). The uni-axial properties of concrete were input in terms of stresses as a tabular function of plastic strains. Because pushover analyses were conducted in the study reported herein to simulate the response of specimens that were subjected to cyclic loading, the reduction in the lateral stiffness of the specimens that occurred due to concrete cracking was accounted for in the analyses based on an equation recommended by Paulay and Priestley (Paulay and Priestley, 1992). The recommended equation is related to the moment of inertia of the uncracked gross cross section.

However, as the cross-sectional dimensions of the specimens could not be modified in the FE model during analysis, the equation was made to be related to the modulus of elasticity of concrete.

3.2.2 Reinforcement

The property of the reinforcing bars was incorporated into the FE models using a standard metal plasticity model. The property of the reinforcing bars was input in terms of stresses as a tabular function of plastic strains. Results of tensile strength tests of the reinforcing bars were used to determine the peak strengths that would be achieved by the longitudinal reinforcing bars in the FE models. The peak strengths to be achieved were interpolated from the tensile strength test stress-strain data, using the average of the peak strains measured during experimental testing of the walls and assuming a bilinear stress-strain relationship. After peak strengths were achieved, the stress within the reinforcing bars was assumed to decline linearly to 1 MPa at the fracture strains that were determined from tensile strength tests (Refer to **Figure 3**). Abaqus interpolates stresses at a given state from the given data and assumes a constant stress for plastic strain magnitudes beyond the last given value.

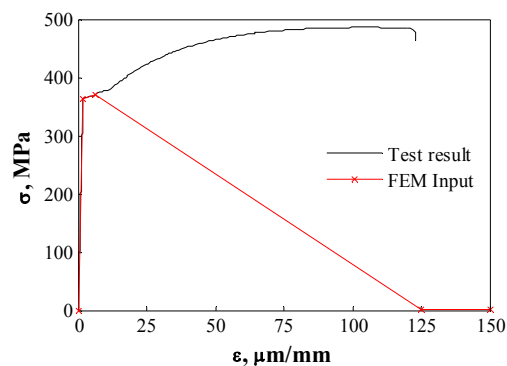


Figure 3. Behaviour of the 10 mm diameter longitudinal reinforcing bar in specimen WPS3

The lengths along the yielding reinforcing bars upon which extension calculations were to be undertaken were not exactly determined from the experimental testing, although single cracks were observed to be formed near to the supports of the test specimens during almost all of the tests. Because linear truss elements were used to model the reinforcing bars in Abaqus, choosing an appropriate length for the elements of the reinforcing bars was vital, as Abaqus assumes a uniform level of stress along the specified element length of a linear element. It was attempted to solve the problem by using cubic elements having a dimension of 10 mm for the concrete and 10 mm long linear truss elements for the longitudinal reinforcement at the bottom and top 50 mm of the walls. From the ensuing analyses, it was found that the mesh needed to be refined further. Reducing the size of the elements of the concrete and reinforcing bars significantly would have provided the desired results. However, refining the mesh further was found to be computationally very expensive and impracticable, and thus, not pursued in this study.

Consequently, the elements of the longitudinal reinforcing bars that were located near to the supports of the walls were made 100 mm long in the FE models, so that the centroid of the elements coincides with the locations where strains in the reinforcing bars were monitored.

3.2.3 Bond between reinforcement and concrete

Special elements available in Abaqus such as the TRANSLATOR element can be employed to model bond stress-slip relationships along concrete – reinforcement interfaces, when relative slip is likely to occur before the tensile strength of the reinforcement is achieved. These elements provide a slot constraint between two nodes, align the local directions of the nodes and permit relative translation along one of the axes as per a predefined function and fully couple the remaining five degrees of freedom. The bond stress-slip behaviour can then be defined using relationships such as those

contained in CEB-FIP Model Code 90 (CEB/FIP, 1990).

From the experimental results it was found that current provisions such as those that are contained in ASCE/SEI 41-06 (ASCE/SEI 41, 2007) and CEB-FIP Model Code 90 (CEB/FIP, 1990) significantly underestimate the bond strength that develops between plain round bars and the surrounding concrete. In addition, simulations of the specimens having spliced bars using TRANSLATOR elements and the bond stress - slip relationship given in CEB-FIP Model Code 90 significantly underestimated the strength of the specimens. Therefore, in the numerical model the bond between concrete and reinforcement for all of the test specimens was set to be perfect.

In the FE model the perfect bond assumption was employed by embedding the reinforcing bars within HOST concrete elements using EMBEDDED ELEMENT option. This method imposes a perfect bond between reinforcement and the surrounding concrete by rigidly connecting the nodes of the reinforcing bars to the nodes of the concrete. In this method, the TENSION STIFFENING option simulates the interaction of the reinforcing bar and the surrounding concrete, like bond slip and dowel action, by modifying the behaviour of plain concrete after failure. The TENSION STIFFENING option also relates the retained tensile stress normal to a crack with the deformation in the direction normal to the crack.

3.2.4 Loading members

Mild steel elastic properties were adopted to describe the materials of the steel loading beam, the cross beams, the high strength bars and the actuator.

3.3 Element types and mesh generation

To model the solid members, only first order hexahedral elements were considered in the analyses, as these elements provide good results for minimum cost in three-dimensional analyses. These brick elements have three degrees of freedom at every node: translations in the nodal x, y, and z directions. Depending on the length to height ratio of the walls, the element interpolation functions of fully integrated first-order elements (C3D8) could not accurately approximate the displacement fields and their derivatives, especially the strain distributions associated with bending, resulting in incorrect shear strains at the integration points. These incorrect shear strains result in false stresses and cause the flexural response of walls to be too stiff, a phenomenon known as shear locking.

To avoid shear locking, either reduced integration elements (C3D8R) or incompatible mode elements (C3D8I) can be used. Employing reduced integration elements is an effective and computationally less expensive option, but multiple numbers of reduced integration elements might be needed across the thickness of a wall to model flexural behaviour adequately. In addition, a uniformly reduced integration can introduce hourglassing, also referred to as zero energy modes, which are non-rigid body motions that lead to no strain or stress at the integration points. Therefore, the option of employing C3D8I elements was also investigated to investigate whether C3D8I elements would provide better results than C3D8R elements.

The term “incompatible” refers to the formulation of C3D8I elements that does not require the derivatives of the displacement fields to be compatible with the displacement interpolation functions (Bower, 2010). Incompatible mode elements use full integration and, hence have no hourglass modes, and yield almost as accurate results as higher-order elements if the elements have a regular hexahedral shape. If the elements are significantly distorted from a cubic shape, their accuracy could be compromised considerably. Incompatible mode elements are computationally less economical than other same-order elements, but are less expensive than higher-order elements. One significant advantage of using C3D8I elements was that these elements can be used in the same mesh with C3D8R elements, with the C3D8I being used only in regions where bending response must be modelled accurately, to reduce computational cost.

A sensitivity study revealed that for the walls discussed herein C3D8R elements with the default

hourglass control option provide good results with the least computational effort. Two elements across the thickness of the walls, a uniform mesh size of 100 mm for the concrete and the reinforcements of the walls and a mesh size of 150 mm for the foundation blocks, the top block and the loading members were observed to yield good results. The reinforcing bars were modelled using the two-node linear truss elements (T3D2). The steel loading beam, the hydraulic jack, the cross beams and the high strength bars were modelled using the two-node linear beam elements (B31).

3.4 Non-linear finite element analyses

Abaqus/Explicit employs a dynamic procedure that was originally developed to model high-speed dynamic problems, but it is also suitable to analyse non-linear quasi-static problems as long as dynamic effects remain suppressed. To inhibit dynamic effects from dominating the response and to insure static response, the loading needs to be applied slowly. However, a slow loading rate is computationally very expensive. The computational cost can be reduced by increasing the loading rate until any further increase no longer results in a static response. A sensitivity study was undertaken to determine the optimum loading rate, and a maximum velocity of 2 mm/s was observed to have resulted in static response for the walls discussed herein. During the simulations, the velocity was ramped up slowly from zero at the beginning of an analysis step to 2 mm/s. Sudden movements were avoided to prevent numerical problems from arising and to prevent dynamic effects from becoming significant.

The computational cost can also be reduced by applying mass scaling to increase the stable time increment. Mass scaling can be achieved by artificially increasing the material density or using the fixed and variable mass scaling options that provide more suitable control of mass scaling of all or specific element sets in a model. When mass scaling is applied, care should be taken to ensure that inertial effects remain insignificant and the kinetic energy produced by the system remains low throughout the analyses when compared to the internal energy. A sensitivity study showed that a fixed mass scaling of 10 applied to all of the elements of the model resulted in static response for the walls discussed herein.

Because the quantity of the longitudinal reinforcement present in the walls was low, the analyses were not significantly affected by the selected values of concrete material parameters. Program default values were adopted for flow potential eccentricity, the ratio K_c and the ratio σ_{bo}/σ_{co} . Variation of these parameters does not affect the response of the walls, as the walls were subjected to in-plane forces only. The value of the parameter ψ (dilation angle), which describes the level of volume change experienced by a concrete mass as concrete cracks and slip occurs along cracked surfaces, can be determined from tri-axial compression tests. However, tri-axial compression tests were not conducted and a suitable value of dilation angle for the model was determined by analysing a series of models with dilation angles varying over their admissible range.

The concrete in compression zones of the walls that were tested experimentally was not confined. Therefore, dilation angle values of as low as 10° were assumed initially, since low dilation angles represent inadequate confinement of concrete. The influence of dilation on the response of the 230 mm thick walls was not significant. However, analyses of the 150 mm thick specimens revealed that dilation angles of as low as 10° significantly overestimate post-elastic stiffness and strength degradation of the test specimens. Dilation angles between 20° and 30° captured the volumetric change occurring at the compression toes of the test specimens reasonably well. It should be noted that dilation does not affect the response of the walls within the elastic range, as it represents plastic distortion.

4 RESULTS OF ANALYSES AND DISCUSSION

The FE analyses were able to predict the overall response of the test specimens reasonably well. Typical response observed during the numerical simulations is presented in **Figure 4**. The response predicted by the simulations was dominated by rocking, as was the response observed during

experimental testing. As presented in **Table 2**, the peak strengths predicted by the simulations were on average within 1% of those determined experimentally. The strength of the walls was predicted to be dictated by the strength of longitudinal reinforcement, a behaviour that was observed during the experimental testing as well.

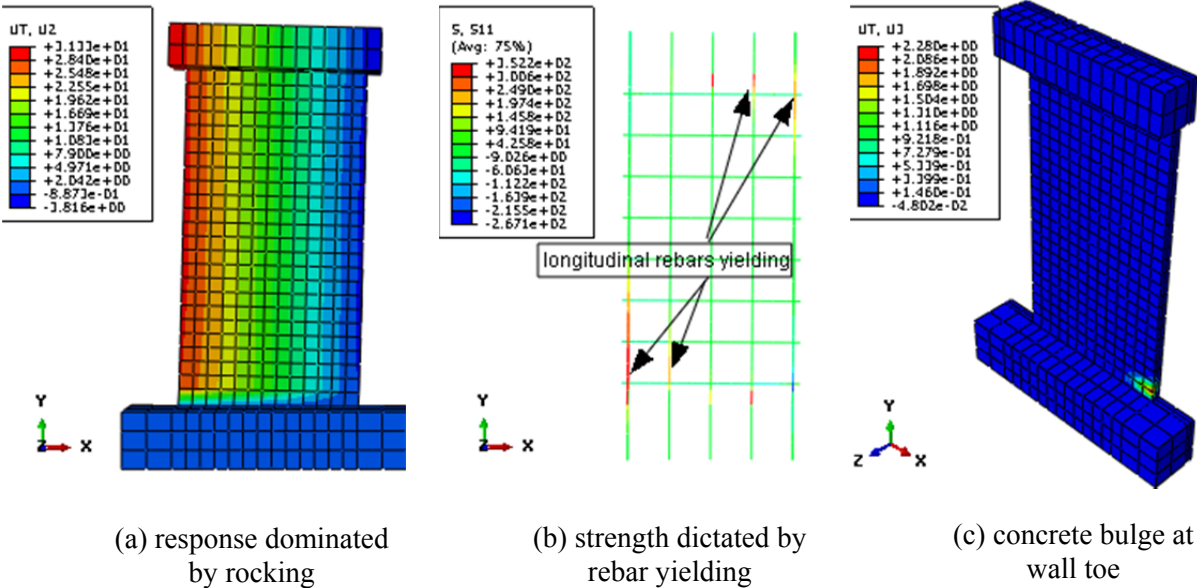


Figure 4. Behaviours observed during the numerical simulations

Lateral-force displacement response determined by the analyses is plotted alongside that determined experimentally in **Figure 5**. Because the experimental response was asymmetric, the results of the analyses are plotted in the quadrant of the lateral force-displacement plot that corresponded with the first loading excursion. Overall, the strength and stiffness degradation predictions for the spine curve were in good agreement with those determined experimentally.

Table 2. Measured and computed peak strengths of the specimens

| Test specimen | l_w mm | h mm | t mm | Compressive axial load kN | V_{Test} kN | V_{FEA} kN | V_{Test} / V_{FEA} |
|--------------------|-------------|-----------|-----------|------------------------------|------------------|-----------------|----------------------|
| WPS3 | 1300 | 2400 | 150 | 0 | 159 | 160 | 0.99 |
| WPS4 | 1300 | 2400 | 230 | 0 | 149 | 154 | 0.97 |
| WPS5 | 1300 | 2400 | 150 | 0 | 199 | 186 | 1.07 |
| WPS6 | 1300 | 2400 | 230 | 0 | 194 | 193 | 1.01 |
| WPS7 | 1300 | 2400 | 150 | 200 | 231 | 233 | 0.99 |
| WPS8 | 1300 | 2400 | 230 | 300 | 271 | 271 | 1.00 |
| WPS9 | 1300 | 2400 | 150 | 200 | 260 | 254 | 1.02 |
| WPS10 | 1300 | 2400 | 230 | 300 | 308 | 301 | 1.02 |
| Average | | | | | | | 1.01 |
| Standard deviation | | | | | | | 0.03 |

Note: 1 mm = 0.0394 in.; 1 kN = 0.225 kips

The simulations significantly overestimated the strength degradation of the two specimens carrying no axial load and having spliced longitudinal reinforcement (specimens WPS5 and WPS6). The overestimation is mainly because the numerical model did not adequately account for the bond stress – slip relationship of plain round reinforcing bars and the surrounding concrete. The model also did not account for the strength produced along the splice lengths due to the dry friction type bond behaviour,

which is the only source of bond strength together with wedging action of dislocated particles after chemical adhesion is overcome. This resistance remains significant even at very large slip values, allowing the reinforcement to carry a considerable amount of force. However, in the numerical model it was assumed that the strength of the reinforcement drops rapidly, immediately after the peak strengths are achieved. When the specimens with lap spliced longitudinal reinforcement had to carry axial loads (specimens WPS7 and WPS8), the bond strength due to friction and wedging action of dislocated particles at the reinforcement-concrete interface was suppressed by the axial loads, and hence, the analyses were able to predict the strength degradations reasonably well.

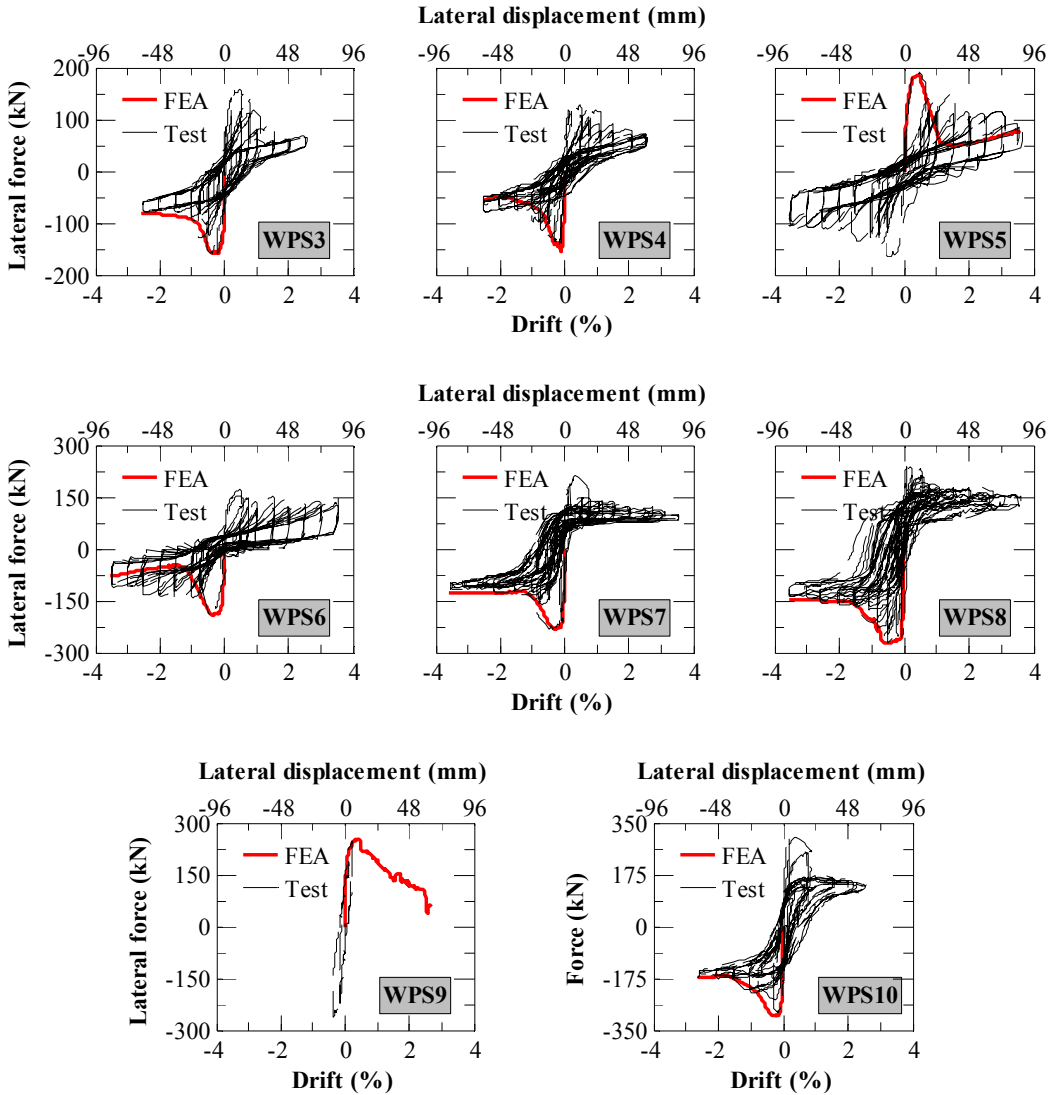


Figure 5. Comparison of test and FEA results

During testing, specimen WPS9 could not achieve the same level of ductility and residual strength exhibited by the other specimens due to rapid loss of axial load carrying capacity. Specimen WPS9 failed in an out-of-plane mode after achieving its predicted yield strength. By modelling the whole specimen, instead of using the half-model that had a symmetry boundary condition that prevents the wall from failing in an out-of-plane mode, an analysis was conducted to investigate whether the out-of-plane failure would be captured. However, the analysis instead predicted a shear – flexure type of failure near the base of the wall that resulted in rapid loss of strength and axial load carrying capacity. The predicted peak strength of the half model is within 2% of that determined experimentally (Refer to Table 2). Had the testing not been discontinued for safety reasons, the predicted lateral force-displacement response could have also closely resembled the experimental response.

5 CONCLUSIONS

A three-dimensional numerical model that was developed to undertake a study on the behaviour of non-ductile RC walls when subjected to earthquake induced lateral forces was presented. The model was verified using data obtained from an experimental program that involved testing of specimens that were replicas of wall segments of an existing building. The peak strengths predicted using the numerical model closely matched those determined during the experimental testing. The model was also able to capture the initial stiffness, the lateral force resisting capacity and the stiffness and strength degradation properties of the test specimens to a good accuracy.

The analyses were not significantly affected by the adopted values of concrete material parameters, as the quantity of the longitudinal reinforcement present in the walls was low. The strengths of the reinforcements during the analyses were limited to the average of those determined using strain gauge data, and thus a study was undertaken to determine a suitable reinforcement strength and reinforcement material model to use when analysing non-ductile RC walls. It was observed that an elasto-plastic material behaviour for the reinforcement of the test specimens reported herein resulted in lower bound lateral force-displacement response that was in good agreement with that determined experimentally.

Simulations of the specimens under cyclic loading were unsuccessful, as buckling of the longitudinal reinforcement was not accounted for in the numerical model. At the time of analyses, methods on how to incorporate the effects of buckling using the FE package employed were not available in the literature. In addition, in order to be able to successfully undertake cyclic analyses of walls having short lap splices, further research is necessary to improve current provisions on the bond stress-slip relationship between plain round reinforcing bars and the surrounding concrete. The current provisions were found to significantly underestimate the bond stress that develops at reinforcement-concrete interfaces.

ACKNOWLEDGEMENT

The authors would like to gratefully acknowledge the financial support provided to this study by the New Zealand Foundation for Research, Science and Technology (FRST) through grant UOAX0411.

REFERENCES

- ACI COMMITTEE 318. (2011). Building code requirements for structural concrete and commentary. Farmington Hills, MI, USA.
- ASCE/SEI 41. (2007). Seismic Rehabilitation of Existing Buildings. Reston, VA, USA: American Society of Civil Engineers.
- BOWER, A. F. (2010). Applied Mechanics of Solids, Taylor & Francis Group.
- CEB/FIP. (1990). CEB-FIP Model Code 1990, International Federation for Structural Concrete (*fib*).
- DASSAULT SYSTÈMES SIMULIA CORP. (2010). ABAQUS Documentation version 6.10.
- DBH. (2004). Building Act 2004. Wellington, New Zealand: Department of Building and Housing.
- GEBREYOHANESS, A. S., CLIFTON, G. C. & BUTTERWORTH, J. W. (2012a). Assessment of the seismic performance of old riveted steel frame - RC wall buildings. *Journal of Constructional Steel Research*. **75**: 1-10.
- GEBREYOHANESS, A. S., CLIFTON, G. C. & BUTTERWORTH, J. W. (2012b). Experimental assessment of inadequately detailed RC wall components. *Manuscript submitted for publication*.
- LEE, J. & FENVES, G. L. (1998). Plastic-damage model for cyclic loading of concrete structures. *Journal of Engineering Mechanics*. **124**: **8**, 892-900.
- LUBLINER, J., OLIVER, J., OLLER, S. & OÑATE, E. (1989). A plastic-damage model for concrete. *International Journal of Solids and Structures*. **25**: **3**, 299-326.
- NZ STANDARDS INSTITUTE. (1935). NZSS 95: New Zealand Standard Building By-Law, Sections I to X. Wellington, New Zealand: NZ Standards Institute.
- PAULAY, T. & PRIESTLEY, M. J. N. (1992). Seismic Design of Reinforced Concrete and Masonry Buildings, John Wiley and Sons, Inc.
- STANDARDS NZ. (2006). NZS 3101:2006 Concrete Structures Standard: Part 1 – The Design of Concrete Structures. Wellington, New Zealand: Standards New Zealand.